

RESEARCH PAPER

Structure-based principles underlying ligand recognition of xanthine-II riboswitch

Xiaochen Xu^{1,2}, Mengqi He¹, Xiaoqing Tai¹, Oianyu Ren³, Xin Shen¹, Chunyan Li¹ & Aiming Ren^{1*}

¹Department of Cardiology, Second Affiliated Hospital of Zhejiang University School of Medicine, Life Sciences Institute, Zhejiang University, Hangzhou 310058, China ²Department of Hematology, The Eighth Affiliated Hospital, Sun Yat-sen University, Shenzhen 518033, China ³Agricultural College, Yangzhou University, Yangzhou 225009, China

*Corresponding author (email: aimingren@zju.edu.cn)

Received 2 August 2024; Accepted 18 November 2024; Published online 24 April 2025

Riboswitches are conserved RNA elements that specifically recognize the cognate metabolites and regulate downstream gene expression involved in the metabolic pathways. To date, two classes of xanthine-responsive riboswitches involved in xanthine homeostasis have been identified. The recently reported xanthine-II riboswitch originates from guanine riboswitch family, featuring a single U-to-G mutation and several nucleotide insertions. Here, we report the complex structure of xanthine-II riboswitch bound to xanthine. The tertiary structure of xanthine-II riboswitch adopts a three-way junction scaffold similar to that of guanine riboswitch. However, the distinctive mutation and insertions in xanthine-II riboswitch facilitate the formation of a highly specific binding pocket for xanthine, distinguishing it from guanine riboswitches. Xanthine is bound in the junction region, forming a base triple with C64 and the mutant nucleotide G37, and is sandwiched by one base pair U8-A38 and one base triple A7-C36-U65. Structural alignment and ligand recognition specificity of the xanthine-II riboswitch are further verified by ligand-binding assays of structure-based mutation using isothermal titration calorimetry. Furthermore, leveraging the ligand specificity of the xanthine-II riboswitch, we develop a highly specific and sensitive biosensor for xanthine detection by fusing xanthine-II riboswitch with Pepper fluorogenic aptamer, highlighting the potential applications of xanthine-II riboswitch in diagnosing diseases related to xanthine metabolism disorders.

riboswitches | xanthine | guanine | tertiary structures | sensing domain | expression platform

INTRODUCTION

Riboswitches are conserved regulatory RNA elements discovered in eukaryotes and archaea, typically located at the 5' non-coding region of genes involved in metabolism, homeostasis and pathogenicity (Breaker, 2012; Mironov et al., 2002; Nahvi et al., 2002; Serganov and Nudler, 2013; Winkler et al., 2002a; Winkler et al., 2002b). Riboswitch usually consists of two tandem domains, the sensing domain and the expression platform, with an overlapping interactive region. The sensing domain recognizes the target metabolite and induces conformational changes by folding into a specific three-dimensional structure. These conformational changes in the sensing domain influence transcription, translation, or splicing of the mRNA at the expression platform, thereby regulating the downstream gene expression (Ariza-Mateos et al., 2021; Breaker, 2012; Jones and Ferré-D'Amaré, 2017; McCown et al., 2017; Pavlova et al., 2019; Serganov and Nudler, 2013). To date, about 60 classes of riboswitches have been identified, recognizing a variety of metabolites, including purines and their derivatives, coenzyme factors, signaling molecules, amino acids and ions (Breaker, 2022). Bioinformatics studies suggest that the known riboswitches may account for only a small fraction of all existent

riboswitches in nature, with many unique structural riboswitches yet to be identified (Greenlee et al., 2018).

Purine and purine derivatives are among the most crucial metabolites, serving as building blocks for DNA and RNA and being essential for energy transfer, signal transduction, and enzyme reactions in all living organisms (Pedley and Benkovic, 2017). Over the past twenty years, various riboswitches that specifically recognize purine or its derivatives metabolites have been discovered (Breaker, 2022). Purine and derivatives riboswitch family is one of the largest and most abundant families. These riboswitches play a significant role in regulating the biosynthesis and transport of purine, thereby maintaining the homeostasis of purine. The ligands recognized by these riboswitches are diverse and abundant, including purines like guanine and adenine, cyclic dinucleotides like c-di-GMP, c-di-AMP and c-GMP-AMP, nucleotides like ADP, ZTP and 2'-dG, and guanine derivatives like xanthine, preQ₁ and ppGpp (Breaker, 2022).

Xanthine is a vital intermediate in purine degradation pathway, which gradually degrades from nucleoside triphosphate, nucleoside diphosphate, nucleoside monophosphate, inosine monophosphate and hypoxanthine, and ultimately being oxidized to uric acid (Lavanya et al., 2016; Pundir and Devi, 2014). Regulation of xanthine levels is essential for maintaining cellular



homeostasis and preventing disorders related to purine metabolism. To date, two classes of riboswitch that specifically recognize xanthine and maintain xanthine homeostasis have been identified (Hamal Dhakal et al., 2022; Yu and Breaker, 2020). The first xanthine-responsive riboswitch, named NMT1 motif, was identified in 2020. Sequence analysis combined with subsequent experiments indicated that it functions as a genetic "OFF" switch to repress the translation of genes associated with purine transport and oxidation in Proteobacteria (Weinberg et al., 2017; Yu and Breaker, 2020). Tertiary structural studies reported by our lab revealed that xanthine-I riboswitch adopts a compact, rod-like helical scaffold with two bulge loops mediating the coaxial stacking of three stems. Xanthine binding pocket is formed by the two internal bulge loops, J1 and J2, through longdistance interactions. Inside the pocket, xanthine is immobilized by key residues and metals that ensure high affinity and selectivity (Xu et al., 2021).

Recently, the second xanthine-responsive riboswitch was discovered, originating from the guanine riboswitch family. In contrast to xanthine-I riboswitch (NMT1 motif), xanthine-II riboswitch functions as a genetic "ON" switch to activate the transcription of genes associated with enzymes like dioxygenase, allantoinase, and xanthine dehydrogenase (Hamal Dhakal et al., 2022). Similar to the guanine riboswitch family, xanthine-II riboswitch adopts a three-way junction scaffold, featuring one large internal bubble and three stems connected to the internal bubble. Unlike the guanine riboswitch family, xanthine-II riboswitch variants have a single U to G mutation, which is involved in the ligand recognition for guanine riboswitches. Additionally, xanthine-II riboswitch variants contain several nucleotide insertions within the internal bubble (Hamal Dhakal et al., 2022).

To investigate the regulation mechanism of xanthine-II riboswitch and elucidate the principles of specific ligand recognition, we determined crystal structure of xanthine-II riboswitch in complex with xanthine at 2.1 Å resolution. The structure revealed a novel and distinct xanthine-recognition mode. We discovered that the unique mutations and insertions facilitate the formation of a highly specific binding pocket for xanthine, distinguishing it from guanine riboswitches. We further verified the structural analysis and ligand recognition specificity of the xanthine-II riboswitch by ligand-binding assays using isothermal titration calorimetry (ITC). Then, we leveraged this specificity by fusing the xanthine-II riboswitch with Pepper fluorogenic aptamer, developing a highly specific and sensitive biosensor for xanthine detection. Overall, our studies reveal the distinct ligand recognition principles of the xanthine-II riboswitch, advance our understanding of riboswitch-mediated gene regulation and provide practical methods to develop RNA-based biosensors with potential applications in diagnosing diseases related to xanthine metabolism disorders.

RESULTS

Constructs design of xanthine-II riboswitch

Xanthine-II riboswitch is a naturally occurring variant belonging to the guanine riboswitch family. Similar to guanine riboswitches, the secondary structure of xanthine-II riboswitch contains an internal junctional loop connecting three stems (Figure S1A) (Hamal Dhakal et al., 2022). Unlike other well-

known purine riboswitches, xanthine-II riboswitch features a key mutation in the highly conserved region, which potentially contributes to ligand recognition. Furthermore, several additional nucleotides are identified in the junction region, with two nucleotides in J2/3 and four nucleotides in J3/1 respectively. Analysis of the consensus models of xanthine-II riboswitch reveals that most nucleotides are highly conserved, particularly in the junction region. Only a few nucleotides within the L2 and L3 loops exhibit notable differences among species (Figure S1A).

Based on the sequence features of xanthine-II riboswitch described above, multiple xanthine-II riboswitch representatives from different species were selected from purine riboswitch family. To facilitate crystallization, we also made additional constructs by introducing mutations in the variable region of the original sequences. The crystal structure of a natural xanthine-II riboswitch derived from Paenibacillus beijingensis strain DSM 24997 in complex with xanthine was determined at a resolution of 2.1 Å. For simplicity, this structure is termed P. beijingensis xanthine-II riboswitch in the following description (Figure 1A-C; Figure S1B). In addition, the complex structure of a mutant xanthine-II riboswitch was determined at a resolution of 2.5 Å. This mutant retains the core sequence of the P. beijingensis xanthine-II riboswitch while incorporating the L2 and L3 loop regions from the Desulfosporosinus youngiae DSM 17734 xanthine-II riboswitch. This structure is referred to xanthine-II-ML2/3 (Figure S1C). Alignment of the global structures between P. beijingensis wild-type xanthine-II riboswitch and xanthine-II-ML2/3 reveals strong similarity, including the variable L2 and L3 regions that contain distinct sequences (Figure S2).

The binding affinity of xanthine-II riboswitch to xanthine was determined using ITC. The wild-type P. beijingensis xanthine-II riboswitch binds to xanthine with a binding affinity $K_{\rm d}$ of (12.1 ± 0.3) $\mu \rm M$. The thermodynamic parameters for the binding were estimated as ΔH =(-15.6 ± 0.1) kcal mol⁻¹ and ΔG =-6.7 kcal mol⁻¹, with a binding stoichiometry approaching 0.6:1 (Figure 1B; Figure S3A). In comparison, the binding affinity of xanthine-II-ML2/3 to xanthine decreases slightly to $K_{\rm d}$ =(25.2 ± 0.7) $\mu \rm M$, with a binding stoichiometry approaching 1:1. The estimated thermodynamic parameters for the binding are ΔH =(-18.7 ± 0.1) kcal mol⁻¹ and ΔG =-6.3 kcal mol⁻¹ (Figure S3B). Consequently, subsequent ITC experiments focused on xanthine-II-ML2/3 for precise stoichiometry measurements.

Overall tertiary structure of xanthine-II riboswitch

In the crystal structure of *P. beijingensis* xanthine-II riboswitch, each asymmetric unit contains two molecules (Mol A and Mol B) arranged in an end-to-end stacking pattern (Figure S4A and B). The Hoogsteen edge of the overhang G1 in Mol A forms two hydrogen bonds with the Watson-Crick edge of the overhang G1' in Mol B, enabling a continuous stacking interaction between the stem P1 of Mol A and stem P1' of Mol B (Figure S4B and C). Except for G1, the conformation of the two RNA molecules is identical, therefore we will focus on Mol A in the following descriptions.

The overall tertiary structure of *P. beijingensis* xanthine-II riboswitch bound with xanthine is shown in cartoon representation and schematically in Figure 1C and D. Consistent with the predicted secondary structure model of xanthine-II riboswitch, three stems P1 (in green), P2 (in orange) and P3 (in slate) are formed and connected by a large junction internal loop (in pink

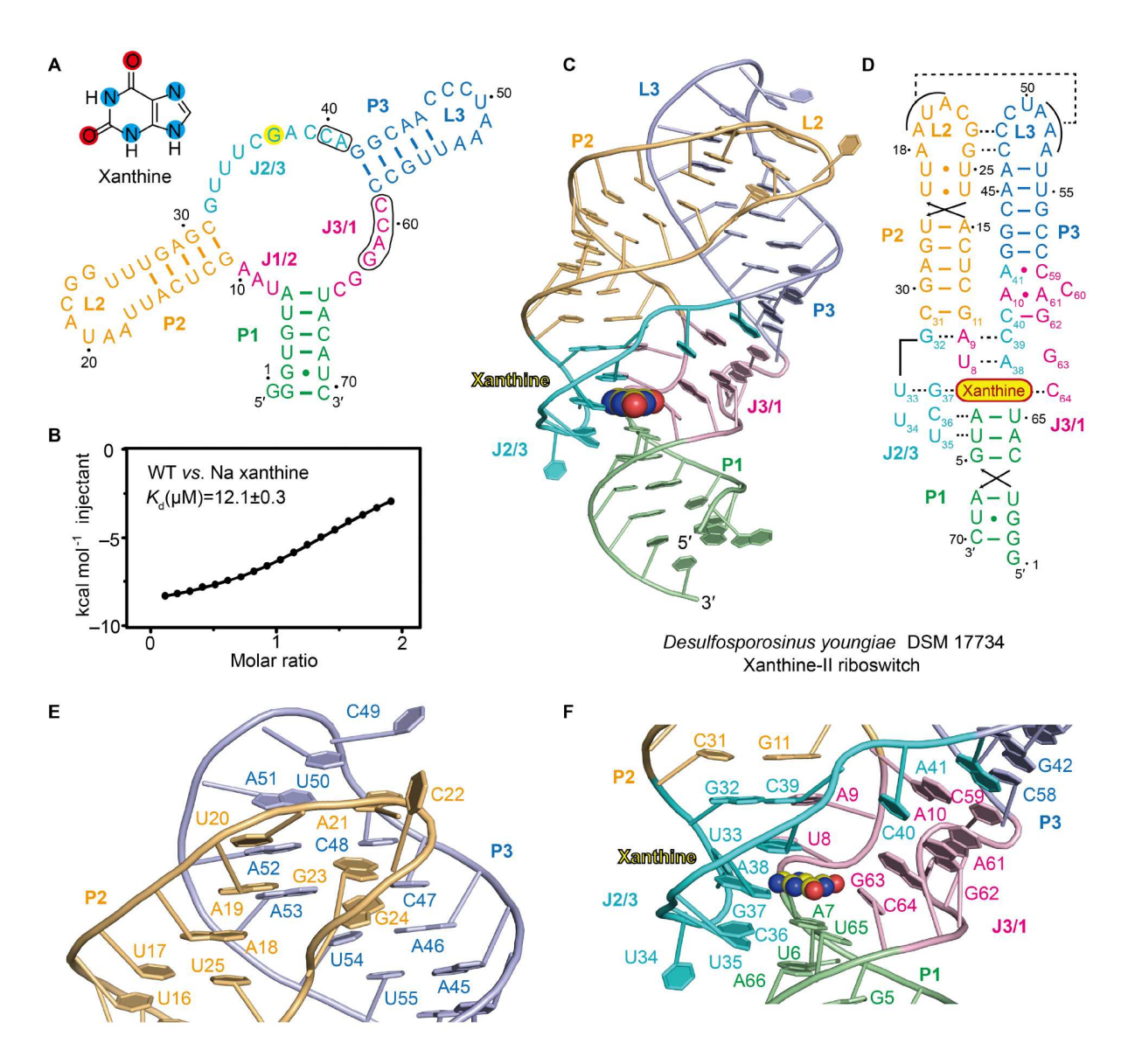


Figure 1. Secondary and tertiary structure of xanthine-II riboswitch bound to xanthine. A, Chemical structure of xanthine (oxygen atoms are highlighted with red shadows, nitrogen atoms are highlighted with blue shadow); and secondary structure of *P. beijingensis* xanthine-II riboswitch. The key mutation (U to G) different from guanine-I riboswitch is labelled with yellow shadow, and the inserted nucleotides different from guanine-I riboswitch are labelled by black rectangle. B, ITC experiment of *P. beijingensis* xanthine-II riboswitch binding to xanthine. Three replicates are shown in Figure S3. C, Cartoon representation of the tertiary structure of *P. beijingensis* xanthine-II riboswitch bound to xanthine (shown in sphere). D, Schematic representation of the tertiary structure of *P. beijingensis* xanthine-II riboswitch, same color code as panel C is used. E, Close-up view of the long-distance interaction between L2 and L3 in *P. beijingensis* xanthine-II riboswitch. F, Structural organization of the junction region J2/3 and J3/1 in *P. beijingensis* xanthine-II riboswitch.

and cyan) (Figure 1C and D). Stem P2 is positioned parallel to stem P3, with the apical loop L2 forming long-distance interactions with L3 (Figure 1C and E). The bottom of stem P2 and P3 exhibits continuous stacking with stem P1, mediated by J2/3 and J3/1 (Figure 1C and F). The ligand xanthine intercalates into the central junction region, forming stacking interaction between stems P1 and P2 (Figure 1C).

The global architecture of the xanthine-II riboswitch adopts a three-way junction conformation similar to that of guanine riboswitch. However, compared to guanine riboswitch, it is notable that the additional nucleotides identified in the junction region of xanthine-II riboswitch form three additional base pairs, including two non-canonical base pairs (A41·C59 and A10·A61) and one canonical base pair (C40-G62). These base

pairs extend stem P3 in xanthine-II riboswitch, differing from the predicted secondary structure model and guanine riboswitch (Figure 1D and F).

As mentioned above, xanthine-II-ML2/3 adopts the same conformation with *P. beijingensis* wild-type xanthine-II riboswitch (Figure S2A–C). Inspection of the apical L2-L3 long-distance interaction region reveals the base paring interaction (U26G) and residual conformation (C22U and C49A) are well maintained in the involved mutations (Figure S2B). Ligand xanthine is consistently positioned in the well-aligned binding cavities of both structures (Figure S2C). These structural alignments reveal that minor variability in L2 and L3 among different species is tolerable for the xanthine-II riboswitch in ligand recognition. This finding is consistent with the consensus

models and our ITC experiments results (Figures S1A and S3).

Long-distance interactions in xanthine-II riboswitch

The long-distance interactions, particularly between L2 and L3 and the well-organized junction region significantly contribute to the folding of the global architecture of the xanthine-II riboswitch. A schematic representation of xanthine-II riboswitch, highlighting these involved nucleotides and specific structural features, is shown in Figure 2A. Stem P2 bends towards stem P3, forming long-distance interactions between L2 and L3, which bring the two stem loops together at the apex of the structure (Figure 1D and E). It is noted that most nucleotides resided in L2 and L3 are involved in base-pairing interaction. A19-A21 from L2 form continuous pairing interaction with A51-A53 from L3, while G23 and G24 from L2 form two Watson-Crick base pairs with C47 and C48 from L3, leaving A18, C22, C49 and U50 unpaired (Figures 1E and 2A-C). The Watson-Crick edge of A19 forms two hydrogen bonds with Hoogsteen edge of A53, the 3-NH of U20 forms one hydrogen bond with N7 of A52, and the Hoogsteen edge of A21 forms two hydrogen bonds with Watson-Crick edge of A51 (Figure 2B). Two canonical Watson-Crick base pairs, G23-C48 and G24-C47, are formed by G23 and G24 from L2, along with C47, C48 from L3, stacking below A21 (Figure 2C). A18 stacks between A19 and two consecutive noncanonical U·U base pairs, U25·U17 and U26·U16, formed in stem P2 (Figure S5A). One hydrogen bond is formed between U17 and U25, while two hydrogen bonds are formed between the Watson-Crick edge of U16 and U26 (Figure S5A). The remaining nucleotides in L2 and L3, including C22, C49 and U50, are flexible without forming any interactions (Figure 1E).

In xanthine-II-ML2/3 structure, the long-distance interaction between L2 and L3 is maintained. The mutant residues C22U and C49A adopt flexible conformation and point outside, while the mutant U26G still forms hydrogen bonds with U16 (Figures S2B and S5B). However, it is notable that U25 and U17 in xanthine-II-ML2/3 slightly shift, forming two hydrogen bonds between their O2 and 3-NH groups, differing from the corresponding interaction in xanthine-II riboswitch (Figure S5B).

The junctional regions J1/2, J2/3 and J3/1 form a complex hydrogen bond network that connects three stems (stem P2, P3 and P1) and participates into the recognition of the xanthine. The most striking feature of the junction region is the tertiary arrangement of the additional nucleotides identified in xanthine-II riboswitch, including C40-A41 in J2/3 and C59-G62 in J3/1. A61 forms a reverse base pair with A10 from J1/2, while C40 and A41 from J2/3 form two base pairs with G62 and C59 from 13/1, sandwiching A61·A10 between them and leaving C60 flipped out without forming any interactions (Figure 2A and D). These long-distance interacting base pairs extend the helix of stem P3. A41 and C59 form a trans Watson-Crick/Watson-Crick base pair and stack below the terminal of stem P3, with 6-NH2 and N1 of A41 forming hydrogen bonds with the N3 and 4-NH2 of C59, respectively (Figure 2A and E). A61 forms a trans Watson-Crick/Hoogsteen base pair with A10, in which the 6-NH2 and the N1 of A61 form hydrogen bond with N7 and 6-NH2 of A10, respectively (Figure 2D and F). C40-G62 forms a canonical cis Watson-Crick base pair, serving as the last extended base pair. The remaining nucleotides in [3/1, G63 and C64, stack continuously from these long-distance base pairs to stem P1 (Figure 2A and D).

In addition to forming long-distance interaction with J3/1, J2/ 3 also forms extra interactions with J1/2 and stem P1, creating several multiple-nucleobases interacting layers that mediate the continuous stacking interaction between stem P1 and P2 (Figure 2A: Figure S5C). Below the terminal base pair (G11-C31) of stem P2. A10 points out from the main chain and pairs with A61. which is further sandwiched between A41 and C40 (Figure S5C). A9 interacts with the sugar edge of G32 through its Watson-Crick edge and forms the first base triple with the canonical Watson-Crick base pair G32-C39, stacking below G11-C31 (Figure 2G). U8 from J1/2 forms a canonical Watson-Crick base pair with A38 from J2/3, serving as the second nucleobase layer below stem P2 (Figure S5D). G37 and U33 interact with each other and both participate in ligand recognition. C36 and U35 interact with the minor groove of stem P1, while U34 points outward without forming any interaction (Figure S5C and D). Notably, C36 forms a base triple with A7-U65, the terminal base pair from stem P1, with the Watson-Crick edge of C36 forming two hydrogen bonds with the O2 and the sugar of U65 (Figure 2H). U35 forms a base triple with U6-A66, the second terminal base pair from stem P1, with the Watson-Crick edge of U35 forming two hydrogen bonds with the N3 and the sugar of A66 (Figure 2I). These two base triples stack below the ligand and compose the last two nucleobase layers in the junction region.

Based on the long-distance interactions observed in the structure, we performed structure-based mutation and ITC experiments to validate these interactions. A19 and U20 form two long-distance base pairs with A53 and A52, while G23 and G24 form two long-distance base pairs with C48 and C47. We designed double mutants A19C/U20C and G23C/G24C to disrupt these long-distance interactions. ITC titration reveals that both mutants lost their binding activity with xanthine (Figure 2J). Point mutants, such as A9C, A10C, G32C and G62C, were also made in the junction region to disrupt the formation of multiple-nucleobase interacting layers. These mutants showed no binding activity to xanthine as well (Figure 2K). Overall, these ITC results confirm the importance of the long-distance interactions in xanthine-II riboswitch binding to xanthine, consistent with the structural analysis.

Binding pocket of xanthine-II riboswitch

The ligand xanthine is bound in the center of the tertiary structure of xanthine-II riboswitch, intercalating between the junction region and stem P1 (Figure 3A; Figure S6A). Several nucleobase stacking layers are formed in the junction region, contributing to the formation of the binding pocket. The involved nucleotides wrap around xanthine completely. Xanthine is sandwiched by base pair U8-A38 and base triple A7-C36-U65 (Figure 3B; Figure S5D). Within the binding pocket, xanthine participates in the formation of a base triple by interacting with G37 from J2/3 and C64 from J3/1. The Watson-Crick edge of C64 forms two hydrogen bonds with the 1-NH and O6 of xanthine, while the Hoogsteen edge of G37 forms two hydrogen bonds with the 3-NH and 9-NH of xanthine, immobilizing it in the binding pocket (Figure 3C). U8 pairs with A38 and stacks upon the bound xanthine. Additionally, U8 recognizes xanthine through its 2'-OH, which forms two hydrogen bonds with O6 and N7 of xanthine (Figure 3C).

Notably, although U33 does not directly interact with xanthine, it plays a crucial role in the formation of the xanthine

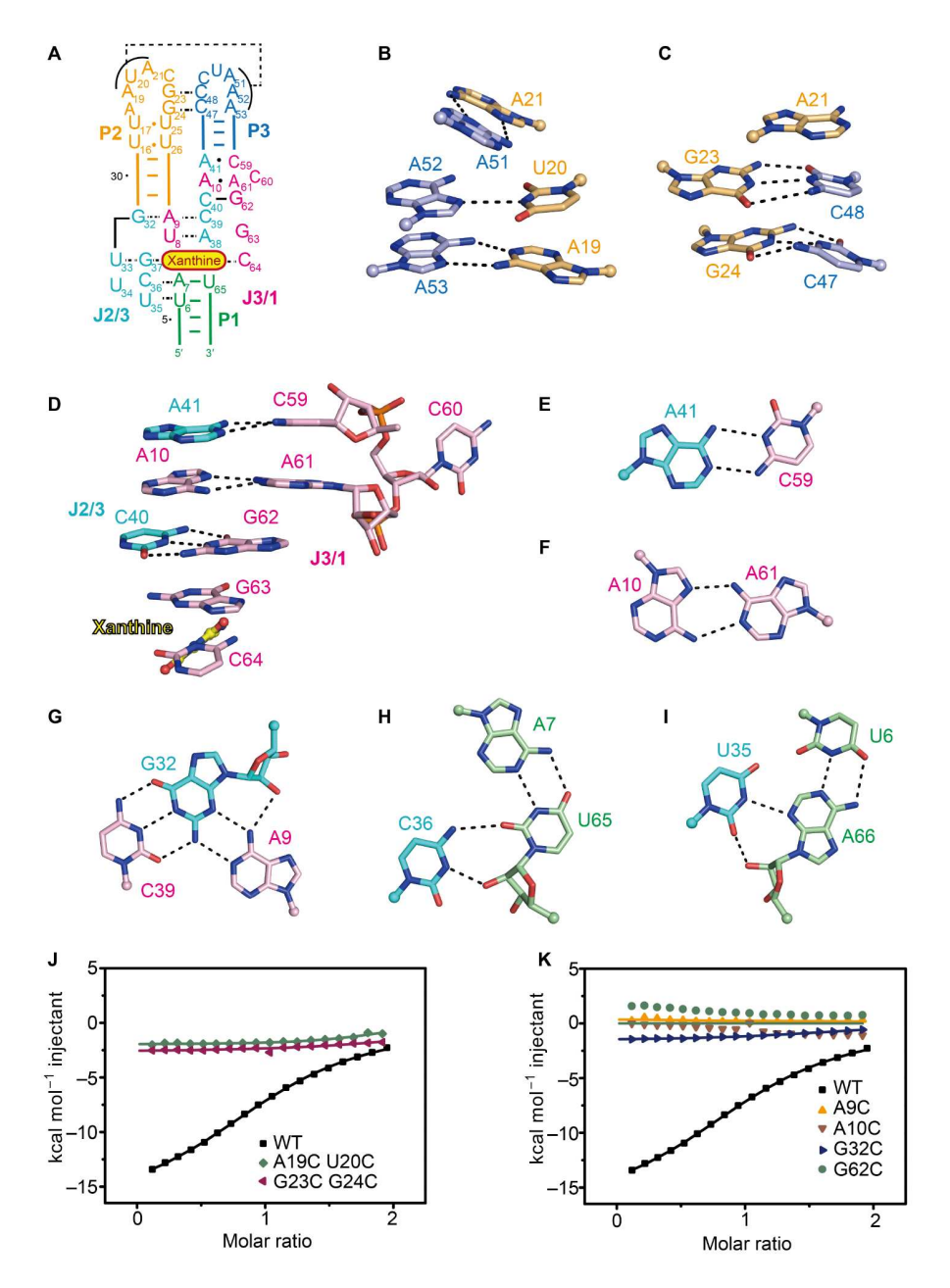


Figure 2. Long distance interactions in xanthine-II riboswitch. A, Schematic secondary structure of xanthine-II riboswitch with the core region highlighted. B, Close-up view of the long-distance interactions between A19–A21 from L2 and A53–A51 from L3. C, Close-up view of the long-distance interactions between G23, G24 from L2 and C47, C48 from L3, which form two canonical G-C base pairs and stack below A21. D, Tertiary arrangement of the additional nucleotides identified in xanthine-II riboswitch, including C40-A41 in J2/3 and C59-G62 in J3/1. E, A41 and C59 form a *trans* Watson-Crick/Watson-Crick base pair with the 6-NH2 and N1 of A41 forming hydrogen bonds with the N3 and 4-NH2 of C59. F, A61 and A10 form a *trans* trans Watson-Crick/Hoogsteen base pair with the 6-NH2 and the N1 of A61 form hydrogen bond with N7 and 6-NH2 of A10. G, Close-up view of the base triple G32-C39-A9 formed by nucleotides from J1/2 and J2/3. A9 interacts with the sugar edge of G32 through its Watson-Crick edge. H, C36 from J2/3 forms a base triple with A7-U65 from stem P1, with the Watson-Crick edge of C36 forming two hydrogen bonds with the Sugar edge of U65. I, U35 from J2/3 forms a base triple with U6-A66 from stem P1, with the Watson-Crick edge of U35 forming two hydrogen bonds with the Sugar edge of U65. I, Overlay of ITC titration heat plot of xanthine-II riboswitch in comparison with mutants concerning nucleotides in Junction region. WT refers to xanthine-II ML2/3 here.

binding pocket. The base of U33 is tilted along the xanthine binding pocket, forming three hydrogen bonds with U35, G37 and A38, thereby stabilizing the nucleobase layers within the binding pocket (Figure 3D). Specifically, its O4 forms one hydrogen bond with the 6-NH2 of A38 from the upper base layer U8-A38, its 3-NH forms one hydrogen bond with the O6 of G37 from the middle base layer G37-C64-xanthine and its O2 forms one hydrogen bond with the 2'-OH of U35 from the lower

base layer U6-A66-U35 (Figure 3D). Additionally, the 2-NH2 of G37 forms one hydrogen bond with the non-bridging phosphate oxygen of C36 from the base layer A7-C36-U65, further reinforcing the stabilization of the binding pocket (Figure 3D).

To evaluate the importance of these nucleobases participating in xanthine recognition by xanthine-II riboswitch, mutants U8A, U33A, G37U and C64G were prepared for ITC experiments (Figure 3E). The mutants that disrupt the specific interactions

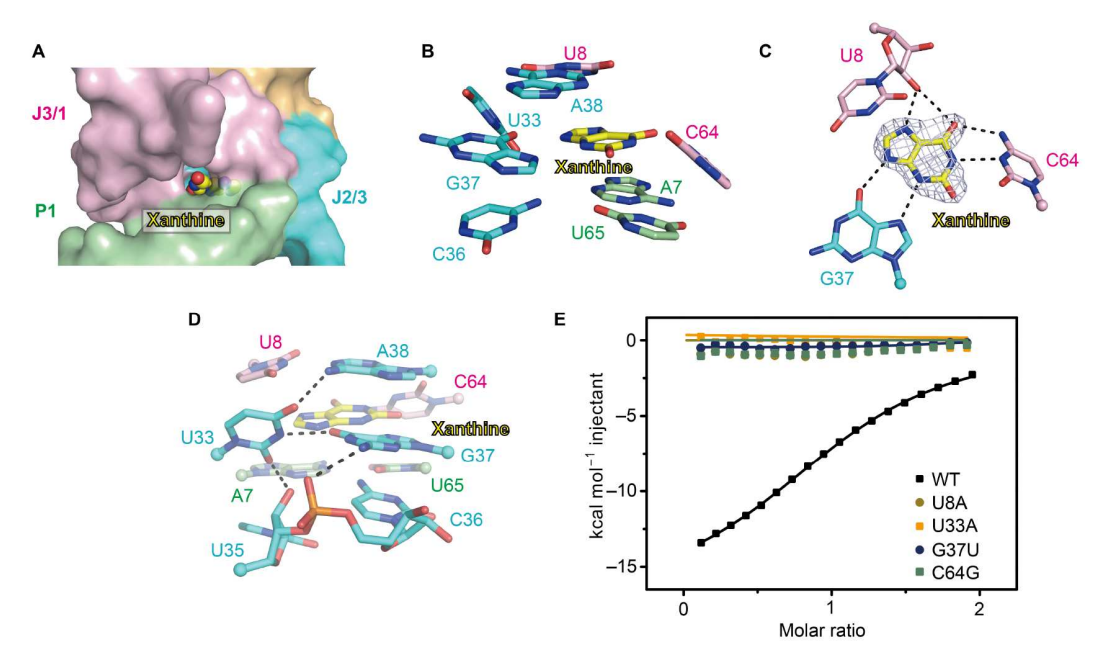


Figure 3. Ligand interactions between xanthine and xanthine-II riboswitch. A, Ligand xanthine (shown in sphere) is bound in the center of the tertiary structure of xanthine-II riboswitch, intercalating between the junction region and stem P1 (shown in surface). B, Xanthine pairs with G37 and C64, and are sandwiched by base pair U8-A38 and base triple A7-C36-U65. C, The Watson-Crick edge of C64 forms two hydrogen bonds with the 1-NH and O6 of xanthine, the Hoogsteen edge of G37 forms two hydrogen bonds with the 3-NH and 9-NH of xanthine, and the sugar of U8 forms two hydrogen bonds with the N7 and O6 of xanthine. D, The base of U33 is tilted along the xanthine binding pocket, forming three hydrogen bonds with U35, G37 and A38. E, Overlay of ITC titration heat plot of xanthine-II riboswitch in comparison with mutants concerning nucleotides in binding pocket. WT refers to xanthine-II ML2/3 here.

with xanthine (G37U and C64G), as well as those affecting the stability of the nucleobase layers (U8A and U33A), lost the binding ability to xanthine (Figure 3E). These results are consistent with what we observed in the xanthine binding pocket (Figure 3D).

Within the binding pocket of xanthine-II riboswitch, two cations are observed (Figure S6A and B). Based on the coordination geometries and the crystallization condition, they are most likely Mg²⁺. M1 and M2 are located between the main chain of U8-A9 and the bases of G62-G63. M1 forms innersphere coordination with O6 of xanthine directly. Besides, it also forms inner-sphere coordination with the 2'-OH of U8, the nonbridging phosphate oxygen of A9 and the 2-NH2 of G63. M2 forms inner-sphere coordination with the non-bridging phosphate oxygen of A9 and several outer-sphere coordination with the O6 and N7 of G62, as well as the O6 of G63 (Figure S6B). In the structure of xanthine-II-ML2/3, the composition of the xanthine-binding pocket and the interaction pattern are same as in P. beijingensis xanthine-II riboswitch (Figure S6C). However, only one cation (M1') is observed in the xanthine-binding pocket of xanthine-II-ML2/3, located in a similar position to M2 in P. beijingensis xanthine-II riboswitch. M1' forms inner-sphere coordination with the non-bridging phosphate oxygen of A9 and 2-NH2 of G62, and several outer-sphere coordination with the 2'-OH of U8, the 2-NH2 of G63 and the N7 of G62 (Figure S6D). Therefore, we speculate that while cations participate in the composition of the xanthine binding pocket of xanthine-II riboswitch, they may not be essential for xanthine recognition.

Specific recognition of xanthine by xanthine-II riboswitch

Since both xanthine-II riboswitch and guanine-I riboswitch belong to purine riboswitch family and employ a similar

architecture, we conducted a thorough examination of their tertiary structures and binding pockets between them. This comparison reveals that each riboswitch has a unique binding mode suitable for recognizing its target ligand. As previously mentioned, xanthine-II riboswitch carries a notable U to G mutation at I2/3 compared to guanine-I riboswitch. In xanthine-II riboswitch, the mutant G (G37) forms two hydrogen bonds with the 3-NH and 9-NH of the ligand xanthine through its Hoogsteen edge. In contrast, U51 forms three hydrogen bonds with the 2-NH2, N3 and 9-NH of the ligand guanine through its Watson-Crick edge in guanine-I riboswitch (PDB: 6UBU) (Figure 4A and B; Figure S7) (Matyjasik et al., 2020). Notably, the 3-NH of xanthine serves as hydrogen bond donor when interacting with N7 of G37, while the N3 of guanine serves as hydrogen bond acceptor when interacting with 3-NH of U51 (Figure 4A and B). In recognizing the Watson-Crick edge of the bound ligand, C64 in xanthine-II riboswitch forms two hydrogen bonds with the O6 and 1-NH of xanthine, while C74 in guanine-I riboswitch forms the canonical base pair interactions with guanine involving three hydrogen bonds. In recognizing the Hoogsteen edge of the ligand, U8 in xanthine-II riboswitch forms two hydrogen bonds with the N7 and O6 of xanthine, while U22 in guanine-I riboswitch forms a single hydrogen bond with the N7 of guanine through its 2'-OH (Figure 4A and B).

In-line probing results reported by Breaker's lab show that the xanthine-II riboswitch specifically binds to xanthine and rejects other purine analogs with similar chemical scaffolds, including guanine (Hamal Dhakal et al., 2022), which is consistent with our structural analysis. In xanthine-II riboswitch, if the bound xanthine is substituted with guanine, the Hoogsteen edge of G37 cannot maintain the interactions with the sugar edge of guanine because the N3 of guanine lacks hydrogen for the hydrogen bond formation, although C64 and U8 can still recognize Watson-

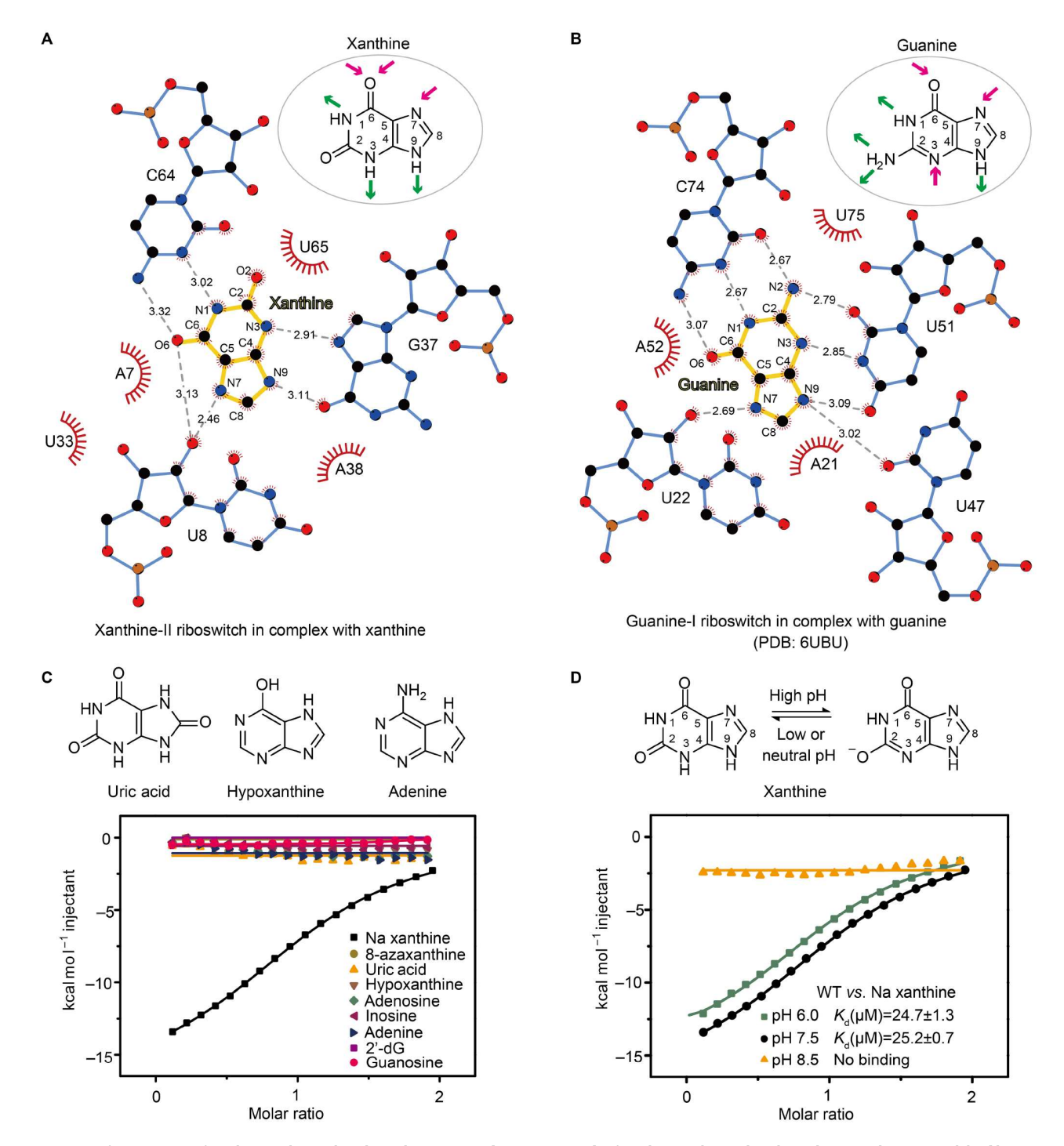


Figure 4. Specific recognition of xanthine-II riboswitch with xanthine. A, Ligand recognition mode of xanthine-II riboswitch with xanthine is immobilized by U8, G37 and C64. B, Ligand recognition mode of guanine-I riboswitch with guanine. Guanine is immobilized by U22, U51 and C74. C, Chemical structure of uric acid, hypoxanthine and adenine. And overlay of ITC titration heat plot of xanthine-II riboswitch with xanthine (in black) and other purine molecules, including 8-azaxanthine, uric acid, hypoxanthine, adenine, adenosine, guanosine, inosine and 2'-dG. D, Protonation equilibria of xanthine. And overlay of integrated fitted heat plots obtained from pH dependence ITC experiments of xanthine-II riboswitch binding to xanthine.

Crick edge and Hoogsteen edge of guanine (Figures 3C and 4A). To verify these speculations, we further perform titrations of xanthine analogs to xanthine-II riboswitch using ITC experiments. The results reveal that the xanthine-II riboswitch has no binding affinity for guanine or other purine analogs, regardless of which atom is replaced or modified, such as C8 replacement (uric

acid and 8-azaxanthine), O2 substitution (hypoxanthine) or addition of the ribose (Figure 4C; Figures S8 and S9A).

It is noted that xanthine undergoes protonation equilibria in different pH solutions (Rogstad et al., 2003). At high pH, xanthine becomes deprotonated, resulting in anionic xanthine with an N3 imine (replacing N3-H in neutral xanthine) and an

anionic oxygen (replacing carbonyl oxygen in neutral xanthine) (Figure 4D). It reminds us that xanthine recognition by the xanthine-II riboswitch may depend on the pH of the buffer. Then we analyzed the potential hydrogen bond patterns for deprotonated xanthine, and compared it with the neutral xanthinebound form. The switch from 3-NH (in neutral xanthine) to N3 imine (in deprotonated xanthine) would disrupt the hydrogen bond between 3-NH and N7 of G37, while the negative charge at the O2 of xanthine may not significantly influence ligand recognition. These analyses suggest that the xanthine-II riboswitch prefers binding to neutral xanthine rather than deprotonated xanthine. To confirm this, we performed ITC experiments in the same buffer system with varying pH values at 6.0, 7.5 and 8.5. The results reveal that the xanthine-II riboswitch shows comparable binding affinities to neutral xanthine in pH 6.0 $(K_d=(24.7\pm1.3) \mu M)$ and pH 7.5 $(K_d=$ (25.2±0.7) μM), while it has no binding ability to deprotonated xanthine in pH 8.5 (Figure 4D; Figure S9B).

Comparison of xanthine recognition pattern

To date, two classes of xanthine-responsive riboswitches have been identified (Hamal Dhakal et al., 2022; Yu and Breaker, 2020). The first xanthine-responsive riboswitch, NMT1 motif, was reported in 2020 and functions as a genetic "OFF" switch to repress the translation of genes predominantly associated with purine transport and oxidation in proteobacteria (Yu and Breaker, 2020). We determined the crystal structures of xanthine-I riboswitch in complex with xanthine or 8-azaxanthine in 2021 (Xu et al., 2021). The xanthine-I riboswitch folds into a compact helical scaffold, with three stems (P1, P2a and P2) exhibiting coaxial stacking. The internal junction [1 and [2 form longdistance interaction that compose the binding pocket (Figure S10A and B). Inside the binding pocket, the ligand xanthine is immobilized by G10 and U40 from J1, A6 from stem P1 and two metal ions, notably Mg²⁺. The ligand xanthine is almost completely encapsulated, with the 1-NH and O2 of xanthine recognized by the Watson-Crick edge of G10, the O2 and 3-NH of xanthine recognized by the Watson-Crick edge of U40, the 7-NH of xanthine recognized by the 2'-OH of A6, the O6 of xanthine coordinated with a metal ion Mg2+ directly, and the N9 of xanthine outer-sphere coordinated with another metal ion Mg²⁺ mediated by a water molecule (Figure 5A). Due to the compensation of these metal ions, the xanthine-I riboswitch can tolerate the binding to both deprotonated xanthine and neutral xanthine with a binding affinity of about 4.4 µM (Xu et al., 2021).

Additionally, a previous study indicated that the guanine-I riboswitch binds to xanthine with significantly weaker affinity than to guanine (Gilbert et al., 2009). In the crystal structure of guanine-I riboswitch in complex with xanthine, the ligand xanthine is immobilized by U22, U51 and C74 in a way similar to that of bound guanine (Figure 5B) (Gilbert et al., 2009; Matyjasik et al., 2020; Serganov et al., 2004). However, the Watson-Crick edge of U51 and C74 each form only two hydrogen bonds with xanthine because of the absence of a hydrogen atom at the O2 of xanthine (Figure 5B), whereas they form three hydrogen bonds with guanine (Figure 4B; Figure S7E). U22 forms an additional hydrogen bond with the N7 of xanthine through its 2'-OH. Notably, the mode of xanthine recognition by guanine-I riboswitch is more similar to that of the xanthine-II riboswitch

recognizing xanthine in our study. ITC experiments indicated that guanine-I riboswitch can bind to the neutral xanthine with an affinity of 39 μ M and exhibits no binding activity to deprotonated xanthine, which is consistent with the findings for xanthine-II riboswitch (Gilbert et al., 2009).

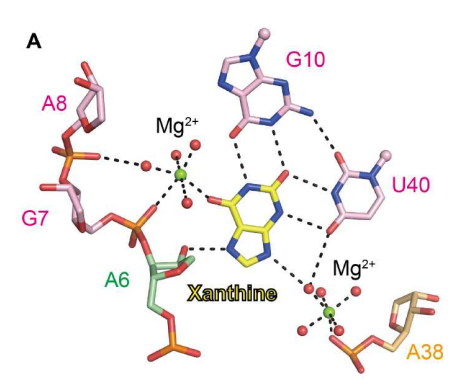
Apart from RNAs, some proteins also possess specific ability to recognize xanthine. Guanine deaminase is an important enzyme that catalyzes the conversion of guanine to xanthine during purine metabolism (Shek et al., 2019). According to the tertiary structure of human guanine deaminase (guaD) in complex with its product xanthine (PDB: 2UZ9), guaD recognizes xanthine through four residues, Gln87, Arg213, Glu243 and His279 (Figure 5C). Gln87 and Arg213 interact with the Hoogsteen edge of xanthine, with Gln87 forming one hydrogen bond with O6 of xanthine and Arg213 forming two hydrogen bonds with O6 and N7 of xanthine. Glu243 and His279 each form one hydrogen bond with the 3-NH and O2 of xanthine, respectively (Figure 5C). It is noteworthy that the 3-NH of xanthine differs from the 3-N of guanine. The specific hydrogen bond interaction involving 3-NH of xanthine may also account for guanine deaminase's ability to discriminate between xanthine and guanine.

Biosensor design for xanthine detection

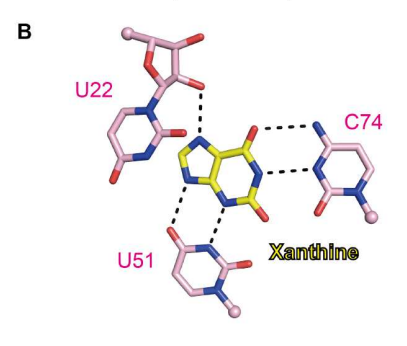
Xanthine is an essential intermediate in the purine degradation pathway, formed by oxidation of hypoxanthine and subsequently oxidized to uric acid (Pundir and Devi, 2014). The level of xanthine is tightly regulated in organisms and serves as an important indicator of abnormal purine disorders, which usually associated with conditions such as xanthinuria, hyperuricemia, gout and urinary tract disease (Pundir and Devi, 2014). Therefore, monitoring xanthine levels is crucial for the diagnosis of many diseases. Since riboswitches recognize their cognate metabolites with high affinity and specificity, they have been adapted into metabolite biosensors by fusing them with fluorescent RNA aptamers. These riboswitch-based metabolite biosensors enable sensitive and specific detection of molecule metabolism in real time, both *in vitro* and *in vivo* (Jaffrey, 2018; Manna et al., 2021; You et al., 2015).

Based on the high specificity of xanthine recognition by xanthine-II riboswitch, we attempted to engineer it into a novel genetically encoded metabolite biosensors through structural combination with Pepper fluorescent aptamer, known for its bright and stable fluorescence, excellent photophysical properties and small size (Figure S11A) (Chen et al., 2019). The tertiary structure of the xanthine-II riboswitch shows that the ligand xanthine is bound in the junction region and stacked upon stem P1, which does not participate in the specific recognition of xanthine (Figure 1C). The tertiary structure of Pepper in complex with the cognate fluorophore HBC (PDB: 7EOH) shows that HBC is recognized by the junction [1 and [2 and stacked between stem P2 and P1, while stem P3 is located at the terminus of the structure, away from the binding pocket, stacking upon stem P2 and connecting to J2 (Figure S11B) (Huang et al., 2021). Based on the structural information, we linked the bottom part of stem P1 from xanthine-II riboswitch and the upper part of stem P3 from Pepper aptamer, retaining both the xanthine recognition module and the fluorescence activation module (Figure 6A).

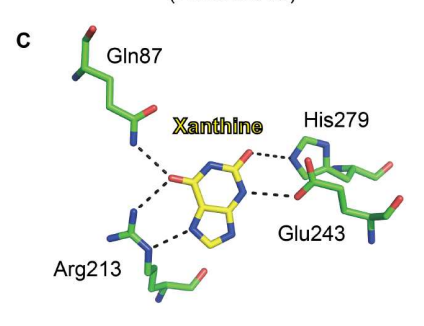
To ensure optimal alignment and interaction between xanthine-II riboswitch and the Pepper fluorescent aptamer, the joint stem was further tested with varying lengths and different



Xanthine-I riboswitch in complex with xanthine (PDB: 7ELR)



Guanine-I riboswitch in complex with xanthine (PDB: 3GAO)



Human guanine deaminase (guaD) in complex with xanthine (PDB: 2UZ9)

Figure 5. Comparison of xanthine recognition pattern. A, Xanthine binding pocket of xanthine-I riboswitch (PDB: 7ELR). Xanthine is immobilized by G10 and U40 from J1, A6 from stem P1 and two metal ions. B, Binding pocket of guanine-I riboswitch bound with xanthine (PDB: 3GAO). Xanthine is immobilized by U22, U51 and C74. C, Binding pocket of guanine deaminase bound with xanthine (PDB: 2UZ9). Xanthine is immobilized by four residues, Gln87, Arg213, Glu243 and His279.

combinations of base pairs (Figure 6A). These recombinant variants were then subjected to fluorescence detection assays to evaluate their ability to produce a strong and specific fluorescence signal in the presence of the same concentration of HBC but with varying concentrations of xanthine. Several recombinant variants, including XP3, XP4, XP3-M1 and XP3-M2, exhibit brighter fluorescence with increased concentration of xanthine (Figure 6B). Although XP3-M1 shows the highest fluorescence signal in the presence of xanthine, it has the drawback of high background fluorescence in the absence of xanthine. XP3 and XP4 display the best performance, showing

about a 10-fold increase in fluorescence in the presence of 1 mmol $\rm L^{-1}$ xanthine compared to the absence of xanthine, and both exhibit a pronounced xanthine-dependent fluorescence increase (Figure 6C; Figure S11C). Furthermore, we examined the ligand recognition specificity of XP3 and XP4. Both exhibit a strong fluorescence response to xanthine and a slight response to guanine, while showing no response to other purine analogs, including 2'-dG, hypoxanthine and uric acid (Figure 6D; Figure S11D). The high specificity and sensitivity of XP3 and XP4 for xanthine make them promising candidates for developing robust and accurate biosensors. These biosensors can be utilized for real-time monitoring of xanthine levels in various biological samples, and could significantly improve disease diagnosis related to xanthine disorder.

DISCUSSION

Riboswitches are a class of regulatory RNA elements that modulate gene expression in response to the binding of specific metabolites. Among them, two xanthine-responsive riboswitches have been identified to date: the xanthine-I riboswitch (NMT1 motif) and the xanthine-II riboswitch. Despite both responding to xanthine, these two riboswitches function differently. The xanthine-I riboswitch acts as a genetic "OFF" switch, repressing the translation of genes associated with purine transport and oxidation (Yu and Breaker, 2020). In contrast, the xanthine-II riboswitch serves as a genetic "ON" switch, activating the transcription of genes involved in purine degradation, such as those encoding dioxygenase, allantoinase, and xanthine dehvdrogenase (Hamal Dhakal et al., 2022). Tertiary structural investigations reveal that these riboswitches adopt different folds and employ distinct recognition patterns for xanthine. The xanthine-II riboswitch, derived from the guanine riboswitch family, features a sophisticated ligand recognition mechanism. It forms a binding pocket at the three-way junction center through interactions among J2/3, stem P1, J1/2, and J3/1. Within this pocket, xanthine is immobilized by interactions with U8, G37, and C64 via the sugar edge, Hoogsteen edge, Watson-Crick edge, respectively. This arrangement ensures high specificity for xanthine binding and highlights the versatility of riboswitch architectures in metabolite recognition.

Comparative analyses between the xanthine-II riboswitch and the guanine riboswitch underscore the impact of minor sequence mutations on ligand specificity. For instance, the guanine riboswitch binds guanine with high affinity, but can also bind xanthine, albeit with significantly weaker affinity (Gilbert et al., 2009). In contrast, Xanthine-II riboswitch, with a single U to G mutation and several nucleotide insertions, has evolved to form a specific recognition site for xanthine. The structural differences, particularly in the hydrogen bonding patterns and the presence of key residues, dictate the specificity of each riboswitch. In guanine riboswitch, U51 and C74 form fewer hydrogen bonds with xanthine compared to guanine, which reduces the binding affinity for xanthine. This comparison illustrates how slight variations in sequence can lead to significant changes in ligand specificity, providing valuable insights for the future exploration and engineering of riboswitches within the same family. In addition, these findings open avenues for the discovery of novel riboswitches. By leveraging the principles of ligand recognition and structural adaptation observed in current riboswitch families, researchers can potentially uncover new riboswitches

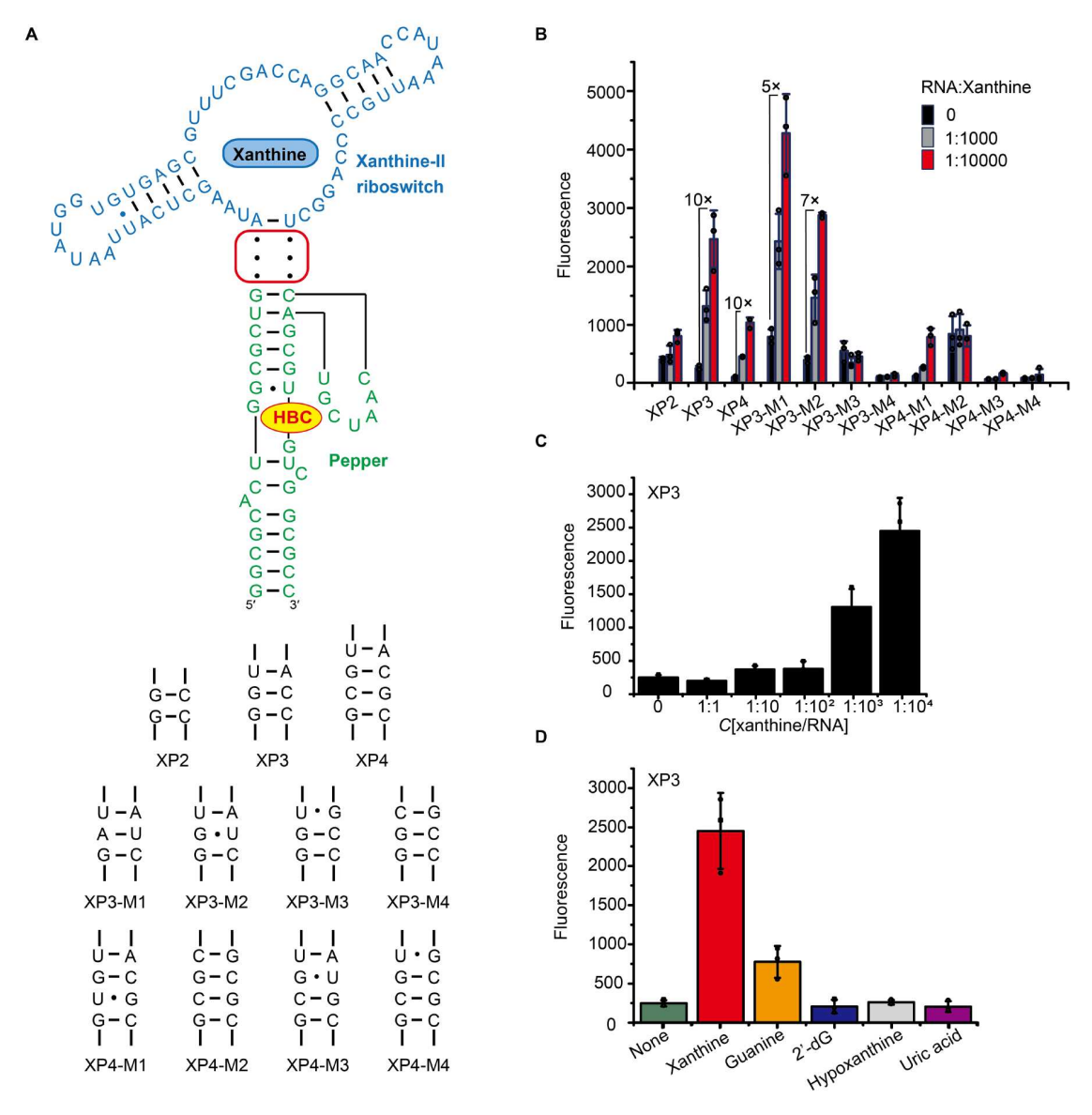


Figure 6. Biosensor design for xanthine detection. A, The schematic diagram of biosensor design. The xanthine-II riboswitch is fused with Pepper fluorescent aptamer and the joint stem was further tested with varying lengths and different combinations of base pairs. B, Fluorescence intensity of recombinant variants in the presence of the same concentration of HBC but with varying concentrations of xanthine. C, Fluorescence intensity of XP3 with different concentration xanthine varying from $0.1 \,\mu$ mol L^{-1} to 1 mmol L^{-1} . The fluorescence of XP3 is brighter with the increased xanthine concentration. D, Fluorescence intensity of XP3 with different purine molecules, including xanthine, guanine, 2'-dG, hypoxanthine and uric acid. XP3 exhibit a strong fluorescence response to xanthine and a slight response to guanine.

with unique regulatory capabilities and ligand specificities.

The high specificity of the xanthine-II riboswitch enables its potential application in developing xanthine biosensors. We fused xanthine-II riboswitch with Pepper fluorogenic aptamer, creating a highly specific and sensitive xanthine biosensor, with potential to detect xanthine levels both *in vitro* and *in vivo*. Xanthine-II riboswitch and its role in biosensor development exemplify the remarkable versatility of riboswitches, serving not only as regulatory elements but also as diagnostic tools. As research in this field progresses, further advancements in riboswitch design and biosensor technology are anticipated. Enhanced understanding of riboswitch structures and their ligand recognition mechanisms will drive the development of more sophisticated and efficient biosensors.

MATERIALS AND METHODS

Chemical compounds

The ligands used in this study were purchased from companies. Xanthine, hypoxanthine, uric acid, adenosine, guanosine, adenine, guanine and inosine were purchased from Yuanye Bio-Technology Co. Ltd. (China). Xanthine sodium salt and 8-azaxanthine monohydrate were purchased from Sigma-Aldrich (USA).

RNA preparation

All RNAs in this study were prepared through *in vitro* transcription (Sun et al., 2019). The sequences of xanthine-II riboswitch

were introduced into pUT-7 plasmid and located between T7 promoter and self-cleavage ribozyme. DNA template was obtained through polymerase chain reaction (PCR) followed by alcohol precipitation. Then *in vitro* transcription was conducted with T7 polymerase, nucleoside triphosphate (NTP) and DNA template at 37°C for 6 h. The product RNA was loaded onto 15% denatured polyacrylamide gel electrophoresis (PAGE), and the bands of target RNA were visualized by an ultraviolet lamp and transferred into 0.5×TAE at 4°C. The extracted RNA solution was purified through alcohol participation and washed with 80% ethanol. After lyophilization, RNA powder was dissolved in diethyl pyrocarbonate (DEPC) treated double-distilled water.

Crystallization

Xanthine-II riboswitch RNAs were diluted to 0.4 mmol L⁻¹ with a crystallization buffer containing 50 mmol L⁻¹ HEPES pH 7.0. 50 mmol L⁻¹ KCl and 5 mmol L⁻¹ MgCl₂ and annealed at 65°C for 5 min followed by incubating on ice for 30 min. Then a final concentration of 6 mmol L-1 xanthine was added into RNA samples and the mixture was incubated on ice for another 30 min. The crystallization screening was performed by mixing 0.2 µL mixture with 0.2 µL reservoir solution purchased from HAMPTON Research using sitting drop vapor diffusion method by a GryPHON-LCP crystallization robot. The high-resolution crystals of xanthine-II riboswitch from Paenibacillus beijingensis strain DSM 24997 grew in the solution containing $0.02 \text{ mol } L^{-1}$ Magnesium chloride, 0.04 mol L⁻¹ Sodium cacodylate pH 5.5. $40\% \text{ v/v (+/-)}-2\text{-Methyl}-2.4\text{-pentanediol}, 0.002 \text{ mol L}^{-1} \text{ Hex-}$ ammine cobalt(III) chloride at 16°C for about 5 d. The highresolution crystals of xanthine-II-ML2/3 grew in the solution containing $0.04~\mathrm{mol}~\mathrm{L}^{-1}$ Lithium chloride, $0.08~\mathrm{mol}~\mathrm{L}^{-1}$ Strontium chloride, 0.02 mol L⁻¹ Magnesium chloride, 0.04 mol L⁻¹ Sodium cacodylate pH 7.0, 30% v/v (+/-)-2-Methyl-2,4pentanediol, $0.012 \text{ mol } L^{-1}$ Spermine tetrahydrochloride at 16°C for about 3 d.

Structure determination

The crystals were stored into liquid nitrogen and carried to Shanghai Synchrotron Radiation Facility (SSRF). All X-ray crystallography diffraction data were collected at the beamline BL19U1, BL18U1 and BL02U1 and processed using HKL3000 (HKL Research, USA). The first determined structure in this study is xanthine-II-ML2/3 and it was determined through molecular replacement using the Phaser MR program in the CCP4 suite (Collaborative Computational Project, 1994) with the crystal structure of guanine-I riboswitch (PDB: 1Y27) as an initial model. The structure of xanthine-II riboswitch from Paenibacillus beijingensis strain DSM 24997 was determined through molecular replacement with the structure of xanthine-II-ML2/3 as the initial model. These structures were further built based on the electron density map including 2Fo-Fc and Fo-Fc maps in COOT (Emsley and Cowtan, 2004) and refined in Phenix (Adams et al., 2010). The ligand xanthine was introduced in the structures at the last several refinements. The X-ray diffraction data and structure refinement statistics are shown in Table S1.

ITC

All ITC experiments in this study were performed on a MicroCal

PEAOITC calorimeter in National Center for Protein Science. Shanghai (NCPSS). The wild-type and mutant RNA samples for ITC were dialyzed in a buffer containing 50 mmol L^{-1} HEPES pH 7.5, 50 mmol L⁻¹ KCl and 10 mmol L⁻¹ MgCl₂ at 4°C overnight and diluted to a final concentration of 1 mmol L^{-1} . Then the RNA was annealed at 65°C for 5 min followed by incubating on ice for 30 min. The ligand xanthine sodium was used to substitute xanthine for better solubility in ITC experiments. All ligands were dissolved in the same buffer and diluted to a final concentration of 100 μmol L⁻¹ except guanine, and guanine was dissolved to a final concentration of 15 µmol L-1. The RNA samples titrated into the cell filled with 200 µL ligand with an initial 0.4 µL injection, followed by 18 serial 2 µL injections. The initial delay was set as 1 min for equilibrium and the interval was set as 2 min between each injection. The reference power was set as $5 \,\mu cal \, s^{-1}$. Besides, the experiments of all RNA samples titrating to buffer were performed for control. The original ITC data were analyzed by the MicroCal PEAQ-ITC Analysis Software using a "one set of sites" binding model and a "single" control type to eliminate the background heat of RNA dilution caused by titration. All the binding constants and thermodynamic values are listed in Table S2.

Biosensor design and identification

The recombinant biosensors were prepared with the above procedure. A final concentration of 0.1 µmol L⁻¹ RNA was diluted in a buffer containing 50 mmol L⁻¹ HEPES pH 7.0. 50 mmol L⁻¹ KCl and 1 mmol L⁻¹ MgCl₂ and annealed at 65°C for 5 min followed by incubating on ice for 30 min. Then different concentration of xanthine was added to RNA varying from 0, $0.1 \, \mu mol \, L^{-1}$, $1 \, \mu mol \, L^{-1}$, $10 \, \mu mol \, L^{-1}$, $100 \, \mu mol \, L^{-1}$ and 1 mmol L^{-1} , and the mixture was incubated on ice for 30 min. Finally, a final concentration of 0.5 µmol L⁻¹ fluorophore HBC was added to the mixture. The fluorescence was detected by a Synergy Neo2 Multi-Mode Microplate Reader (BioTek, USA) with an excitation wavelength of 485 nm and an emission wavelength of 530 nm for HBC after another 30 min. For the specificity detection, a final concentration of 1 mmol L^{-1} xanthine, guanine, 2'-dG, hypoxanthine and uric acid was added into the annealed RNA respectively. All fluorescence experiments were repeated three times independently.

Data availability

Atomic coordinates and structure factors for the reported crystal structures of *P. beijingensis* Xanthine-II riboswitch in complex with Xanthine and xanthine-II-ML2/3 riboswitch have been deposited with the Protein Data bank (www.rcsb.org) under accession numbers 9IWF (*P. beijingensis* Xanthine-II riboswitch structure) and 9IWG (xanthine-II-ML2/3 riboswitch structure), respectively. All study data are included in the article or Supplementary Materials.

Compliance and ethics

The authors declare that they have no conflict of interest.

Acknowledgement

This work was supported by the National Key Research and Development Project of China (2021YFC2300300, 2023YFC2604300) and the National Natural Science Foundation of China (32325029, 91940302, 91640104). We thank the staff members of the Large-scale Protein Preparation System, BL-17B, BL-17U1, BL18U1, and BL-19U1 beamlines at the National Facility

for Protein Science in Shanghai (NFPS), Zhangjiang Lab, China for providing technical support and assistance in data collection and analysis.

Supporting information

The supporting information is available online at https://doi.org/10.1007/s11427-024-2800-0. The supporting materials are published as submitted, without typesetting or editing. The responsibility for scientific accuracy and content remains entirely with the authors.

Open Access

This article is licensed under a Creative Commons Attribution 4.0 International License, which permits use, sharing, adaptation, distribution and reproduction in any medium or format, as long as you give appropriate credit to the original author(s) and the source, provide a link to the Creative Commons licence, and indicate if changes were made. The images or other third party material in this article are included in the article's Creative Commons licence, unless indiparty otherwise in a credit line to the material. If material is not included in the article's Creative Commons licence and your intended use is not permitted by statutory regulation or exceeds the permitted use, you will need to obtain permission directly from the copyright holder. To view a copy of this licence, visit https://creativecommons.org/licenses/by/4.0/.

References

- Adams, P.D., Afonine, P.V., Bunkóczi, G., Chen, V.B., Davis, I.W., Echols, N., Headd, J. J., Hung, L.W., Kapral, G.J., Grosse-Kunstleve, R.W., et al. (2010). PHENIX: a comprehensive Python-based system for macromolecular structure solution. Acta Crystlogr D Biol Crystlogr 66, 213–221.
- Ariza-Mateos, A., Nuthanakanti, A., and Serganov, A. (2021). Riboswitch mechanisms: new tricks for an old dog. Biochem Moscow 86, 962–975.
- Breaker, R.R. (2012). Riboswitches and the RNA world. Cold Spring Harb Perspect Biol 4, a003566.
- Breaker, R.R. (2022). The biochemical landscape of riboswitch ligands. Biochemistry 61, 137–149.
- Chen, X., Zhang, D., Su, N., Bao, B., Xie, X., Zuo, F., Yang, L., Wang, H., Jiang, L., Lin, Q., et al. (2019). Visualizing RNA dynamics in live cells with bright and stable fluorescent RNAs. Nat Biotechnol 37, 1287–1293.
- Collaborative Computational Project, N (1994). The CCP4 suite: programs for protein crystallography. Acta Crystlogr D Biol Crystlogr 50, 760–763.
- Emsley, P., and Cowtan, K. (2004). Coot: model-building tools for molecular graphics. Acta Crystlogr D Biol Crystlogr 60, 2126–2132.
- Gilbert, S.D., Reyes, F.E., Edwards, A.L., and Batey, R.T. (2009). Adaptive ligand binding by the purine riboswitch in the recognition of guanine and adenine analogs. Structure 17, 857–868.
- Greenlee, E.B., Stav, S., Atilho, R.M., Brewer, K.I., Harris, K.A., Malkowski, S.N., Mirihana Arachchilage, G., Perkins, K.R., Sherlock, M.E., and Breaker, R.R. (2018). Challenges of ligand identification for the second wave of orphan riboswitch candidates. RNA Biol 15, 377–390.
- Hamal Dhakal, S., Panchapakesan, S.S.S., Slattery, P., Roth, A., and Breaker, R.R. (2022). Variants of the guanine riboswitch class exhibit altered ligand specificities for xanthine, guanine, or 2'-deoxyguanosine. Proc Natl Acad Sci USA 119, e2120246119.
- Huang, K., Chen, X., Li, C., Song, Q., Li, H., Zhu, L., Yang, Y., and Ren, A. (2021). Structure-based investigation of fluorogenic Pepper aptamer. Nat Chem Biol 17, 1289–1295.
- Jaffrey, S.R. (2018). RNA-based fluorescent biosensors for detecting metabolites in vitro and in living cells. Adv Pharmacol 82, 187–203.
- Jones, C.P., and Ferré-D'Amaré, A.R. (2017). Long-range interactions in riboswitch control of gene expression. Annu Rev Biophys 46, 455–481.

- Lavanya, N., Sekar, C., Murugan, R., and Ravi, G. (2016). An ultrasensitive electrochemical sensor for simultaneous determination of xanthine, hypoxanthine and uric acid based on Co doped CeO_2 nanoparticles. Mater Sci Eng-C 65, 278–286.
- Manna, S., Kellenberger, C.A., Hallberg, Z.F., and Hammond, M.C. (2021). Live cell imaging using riboswitch-Spinach tRNA fusions as metabolite-sensing fluorescent biosensors. In: Ponchon, L., ed. RNA Scaffolds. Methods in Molecular Biology. New York: Humana. 121–140.
- Matyjasik, M.M., Hall, S.D., and Batey, R.T. (2020). High affinity binding of N₂-modified guanine derivatives significantly disrupts the ligand binding pocket of the guanine riboswitch. Molecules 25, 2295.
- McCown, P.J., Corbino, K.A., Stav, S., Sherlock, M.E., and Breaker, R.R. (2017). Riboswitch diversity and distribution, RNA 23, 995–1011.
- Mironov, A.S., Gusarov, I., Rafikov, R., Lopez, L.E., Shatalin, K., Kreneva, R.A., Perumov, D.A., and Nudler, E. (2002). Sensing small molecules by nascent RNA: a mechanism to control transcription in bacteria. Cell 111, 747–756.
- Nahvi, A., Sudarsan, N., Ebert, M.S., Zou, X., Brown, K.L., and Breaker, R.R. (2002). Genetic control by a metabolite binding mRNA. Chem Biol 9, 1043–1049.
- Pavlova, N., Kaloudas, D., and Penchovsky, R. (2019). Riboswitch distribution, structure, and function in bacteria. Gene 708, 38–48.
- Pedley, A.M., and Benkovic, S.J. (2017). A new view into the regulation of purine metabolism: the purinosome. Trends Biochem Sci 42, 141–154.
- Pundir, C.S., and Devi, R. (2014). Biosensing methods for xanthine determination: a review. Enzyme Microb Tech 57, 55–62.
- Rogstad, K.N., Jang, Y.H., Sowers, L.C., and Goddard, W.A. (2003). First principles calculations of the pK_a values and tautomers of isoguanine and xanthine. Chem Res Toxicol 16, 1455–1462.
- Serganov, A., and Nudler, E. (2013). A decade of riboswitches. Cell 152, 17-24.
- Serganov, A., Yuan, Y.R., Pikovskaya, O., Polonskaia, A., Malinina, L., Phan, A.T., Hobartner, C., Micura, R., Breaker, R.R., and Patel, D.J. (2004). Structural basis for discriminative regulation of gene expression by adenine- and guanine-sensing mRNAs. Chem Biol 11, 1729–1741.
- Shek, R., Hilaire, T., Sim, J., and French, J.B. (2019). Structural determinants for substrate selectivity in guanine deaminase enzymes of the amidohydrolase superfamily. Biochemistry 58, 3280–3292.
- Sun, A., Huang, K., Zheng, L., and Ren, A. (2019). Strategies for understanding RNA recognition by X-ray crystallography and NMR methods. Methods Enzymol 623, 229–248.
- Weinberg, Z., Lünse, C.E., Corbino, K.A., Ames, T.D., Nelson, J.W., Roth, A., Perkins, K.R., Sherlock, M.E., and Breaker, R.R. (2017). Detection of 224 candidate structured RNAs by comparative analysis of specific subsets of intergenic regions. Nucleic Acids Res 45, 10811–10823.
- Winkler, W., Nahvi, A., and Breaker, R.R. (2002a). Thiamine derivatives bind messenger RNAs directly to regulate bacterial gene expression. Nature 419, 952– 956.
- Winkler, W.C., Cohen-Chalamish, S., and Breaker, R.R. (2002b). An mRNA structure that controls gene expression by binding FMN. Proc Natl Acad Sci USA 99, 15908– 15913
- Xu, X., Egger, M., Chen, H., Bartosik, K., Micura, R., and Ren, A. (2021). Insights into xanthine riboswitch structure and metal ion-mediated ligand recognition. Nucleic Acids Res 49, 7139–7153.
- You, M., Litke, J.L., and Jaffrey, S.R. (2015). Imaging metabolite dynamics in living cells using a Spinach-based riboswitch. Proc Natl Acad Sci USA 112, E2756– E2765.
- Yu, D., and Breaker, R.R. (2020). A bacterial riboswitch class senses xanthine and uric acid to regulate genes associated with purine oxidation. RNA 26, 960–968.